Received: 13 October 2023 | Revised: 8 December 2023 | Accepted: 4 January 2024

High Voltage

DOI: 10.1049/hve2.12434

ORIGINAL RESEARCH

Experimental qualification and sensitivity study of antipodal patch antenna structures for orientation independent detection of partial discharges

Kerstin Friebe | **Frank Jenau**

TU Dortmund University, Institute of High Voltage Engineering, Dortmund, Germany

Correspondence
Kerstin Friebe.
Email: kerstin.friebe@tu-dortmund.de

Associate Editor: Fuping Zeng

Funding information
Technische Universität Dortmund

Abstract

Partial discharge diagnosis is an important part of monitoring and diagnosing components of the power transmission system. Four different patch antenna structures for the detection of partial discharges are investigated. These patch antennas, which are realisable in a variety of geometric structures, are already the subject of research. They offer the advantage of contactless detection without intervention in the test object or the measuring circuit, and also offer the possibility of alignment independent detection compared to directional antennas. However, it is important and required to examine different structures extensively at the same measurement setup and to compare their performance. To achieve this, four different configurations of patch antenna structures based on basic geometries all in antipodal design are realised: a logarithmic periodic structure, a Hilbert fractal structure and two tapered slot antennas. They are exposed to the same conditions on a special and unique measurement setup. As the main aspect, the performance of orientation independent detection of partial discharges patch antennas with varying distance and rotation in relation to the partial discharge source as well as the operating bandwidth is examined. To rate the structures, an evaluation scheme is created and a sensitivity matrix is generated.

1 | INTRODUCTION TO DETECTION OF PARTIAL DISCHARGES

In the context of partial discharge (PD) diagnosis, various methods for detection of PD are established and are the subject of current research. Essential aspects are introduced in the following.

1.1 | PD measuring circuit according to IEC 60270

The PD measurement method according to IEC 60270 [1] allows the determination of the appearing charge by coupling out the PD pulses by using a coupling capacitor. The charge is determined by the voltage dip caused by the final charge current. For multiphase equipment, several coupling capacitors are required according to the number of phases. As the operating voltage increases, the dimensions and cost of the coupling capacitors also increase. In addition, a coupling quadripole (CQ) is required, which is connected to the measuring device. To determine the appearing charge in this method a calibration with defined charge pulses is necessary. Usually the signals are acquired with bandwidths ≤900 kHz and centre frequencies ≤1 MHz [1–4].

1.2 | Electromagentic PD measurement methods

PD pulses generate electromagnetic waves whose propagation is describable by Maxwell's equations. Depending on the propagation medium of the signal, there are differences in propagation velocity and absorption. Depending on the type of

PD and the medium of emission, the frequency range of the PD pulse is in the range of a few 100 MHz—the so-called VHF range—to a few GHz—the so-called UHF range. Particularly in oil-insulated transformers or gas-insulated switchgear, the PD pulses have substantial components in the GHz range [2, 3].

1.3 | PD acquisition with patch antenna structures

One option within the electromagnetic detection methods is the detection of PD with special antenna structures, the so-called patch antennas or also called stripline antennas. Here, geometric copper structures (so-called patches) are applied to a dielectric substrate. A copper structure is also applied to the back of the substrate, which serves as the opposite pole. Due to the dielectric substrate, the antenna structure is detuned compared to a classical antenna and the necessary dimensions determined by the wavelengths of the frequency range are shortened. Advantages are the high bandwidths which are realisable with small structures at the same time as well as a basically possible omnidirectional characteristic.

In principle, it is possible to realise the structures known from classical antenna designs. In ref. [5], the basic laws of a logarithmic periodic directional antenna structure are applied to a patch structure and sensitivity studies are performed using an FEM tool while varying the parameters of the geometric dimensions. It is implemented antipodally to approximate an omnidirectional radiation pattern. Depending on the detailed structure, working frequency bands in the range of about 5.0–7.5 GHz are obtained. Criteria for defining the working frequency band are a standing wave ratio (VSWR) of <2 and a return loss (RL) of <-10 dB.

In ref. [6], a tapered slot structure similar to the Vivaldi antennas is realised and adapted in several modification steps to a bandwidth relevant for PD measurement, with the aim of reducing the RL over a larger frequency band. This results in a bandwidth of 760 MHz–3 GHz.

Also simple round patch structures allow PD detection. In ref. [7], a round patch structure is realised and characteristics such as VSWR and RL are determined by simulations using an FEM programme. This results in a working frequency band of 1.2–3 GHz, which is defined by a VSWR of <2 and a RL of <-10 dB. Due to a reduced ground plane on the backside, an approximation to an omnidirectional characteristic is obtained, which also extends to the backside of the sensor. In ref. [8], a circular patch structure is realised and implemented in an FEM model of a GIS. Considering an RL of <-10 dB as a criterion, a working frequency band of 0.7 MHz–3 GHz GHz is obtained. Circular structures as studied in ref. [9] are also suitable for PD detection. Here, an Archimedean spiral structure is used to capture three different PD species in oil. Considering a VSWR of <2, a working frequency band of 1.2–3 GHz is given.

A special form are fractal structures, which are characterised by the fact that the structures repeat within themselves in different scales and thus allow a high bandwidth. In ref. [10] two patch antennas of different structure are presented for PD detection. One is a Hilbert fractal with a bandwidth of 0.5–0.9 GHz and the other is a loop structure with a bandwidth of 0.1–0.7 GHz. The working bandwidth is determined by a VSWR of <5. The radiation characteristic is focused on the front side of the structure. Three different types of PD are experimentally detected with the structures and its power spectrum in the frequency domain is investigated. In ref. [11], a loop structure is investigated versus an HFCT. Both are introduced into the grounding branch. For the loop structure, considering a VSWR of <2 and an RL of <-10 dB, a working frequency band of 0.745–1.5 GHz is obtained. In ref. [12], three different types of Hilbert fractals are used to measure three different PD species in an oil-insulated system. The structures differ in the composition of 4th order Hilbert fractals. A working frequency band of 0.5–4.0 GHz is realised. An RL of <-10 dB is set as the criterion for determining the working frequency band. The radiation pattern here also focuses on the front side of the structure. In ref. [13], a 2nd order Hilbert fractal with a parasitic conduction is modified and combined into a stacked structure. The structure is reproduced in an FEM model and tested on a measurement setup with two different PD classes. The working frequency band here is found to be 450 MHz–1 GHz using a VSWR of <5 for determination. In ref. [14], a Peano fractal structure is developed for PD detection at a gas-insulated switchgear. Through simulations and experimental tests, a working frequency band of 300 MHz–3 GHz is obtained. The criterion used is a VSWR of <2. In addition, an ellipsoidal radiation characteristic is obtained.

In ref. [15], a bowtie antenna with centre cutout is developed. Using simulations and experimental studies on a PD measurement setup, a working frequency band of 1.35–1.72 GHz is obtained considering an RL of <-10 dB. In ref. [16], a combination of dipole and bowtie structure is developed for measuring PD in gas-insulated switchgear and compared with a simple dipole structure and a simple bowtie structure. Using simulations, considering the criteria of a VSWR of <2 and an RL of <-10 dB, a working frequency band of 0.8–0.95 GHz or 0.6–1.2 GHz is given.

In this work, four different patch antenna structures are implemented antipodally based on the literature, whereby the hilbert fractal geometry is optimised with regard to an antipodal structure and simultaneous impedance matching. A bandwidth of 0.3–3 GHz is taken as the target bandwidth. In addition, a measurement setup is used to carry out extensive investigations into the orientation independent detection of PD. This unique measurement setup enables triggering on a cable-bound PD signal and thus isolated recording of the PD and subsequent averaging over several pulses to counter measurement uncertainties. It also ensures a constant comparable charge amount. In this study, standardised measurement conditions for different structures are created and extensive

studies on the performance of alignment independent detection are carried out.

2 | METHODICAL APPROACH

As shown in Figure 1, first sensor structures that differ in geometric and physical properties are designed and then their suitability for PD measurement is investigated within experimental investigation. On the one hand, antenna parameters are determined to ensure the working frequency bandwidth and, on the other hand, series of measurements are performed under real conditions to detect PD. Then, the sensors are evaluated with regard to their suitability for PD detection using the measurement data and evaluation criteria.

In the context of the investigations, four different are realised and compared. Target bandwidth is a range of 300 MHz–3 GHz. This broadband detection is desirable in terms of further processing for classification of PD via features such as charge amount and frequency spectrum. The sensor structures differ in their geometry of the copper layer. A logarithmic periodic structure modified from the classical broadband directional logarithmic periodic antenna, a Hilbert structure and two tapered slot structures are realised. All of them have an antipodal structure, which enables orientation independent PD detection. The logarithmic periodic structure represents an electric dipole structure. The special feature of the Hilbert structure is the frontside realisation as an electrical antenna in the form of copper conductor strips and the backside design as a slot antenna inverse to the front side. The tapered slot structures represent the class of slot antennas.

The VSWR is determined for all sensors to characterise the working bandwidth of antenna structures. For patch antennas, the bandwidth is limited by the frequency dependence of their input impedance. The misfit between resonant frequencies causes a ripple on the feed line [17]. A VSWR of 1 corresponds to a complete fit. A VSWR (<2) is used as the evaluation criterion to determine the working frequency band of the designed sensors.

In addition to the determination the antenna parameters, the sensors are tested under real conditions for their suitability for detecting PD. For this purpose, PD are generated in a measurement cell at a needle plane configuration. The test setup ensures that a comparable charge level is set for each measurement series. For this purpose, the DC voltage is adjusted in such a way that a constant amount of charge is achieved. In addition, the test setup enables the sequential recording of the PD pulses and thus an averaging over 1000 pulses in this case. The sensor is positioned at different distances as well as varying rotation and orientation in relation to the measuring cell within the scope of the verification of the suitability for orientation independent PD detection. The rotation takes place on the one hand around the z-axis and on the other hand around the y-axis. This corresponds to a polarisation measurement around the respective axis. The orientation first rotates around the y-axis and then around the x-axis. This represents an alignment of any kind to the PD source. 1000 PD are recorded at each position and an average $s_{z,i}(t)$ of the PD signal is calculated. Even though stochastic interference is partially averaged out, the signal still has interference components. Therefore, 1000 measurements of the interference level $z_i(t)$ are also acquired at each position. In Figure 2, the evaluation process using the measurement data is shown. The evaluation criterion of the signal to noise ratio (SNR) is calculated by

$$\begin{aligned} \mathrm{SNR}_{\mathrm{dB}} &= 10{\cdot}\log\left(\frac{\sum_{i=1}^{n} s_i(t)^2}{\sum_{i=1}^{n} z_i(t)^2}\right) \\ &= 10{\cdot}\log\left(\frac{\sum_{i=1}^{n} \left(s_{z,i}(t) - z_i(t)\right)^2}{\sum_{i=1}^{n} z_i(t)^2}\right). \end{aligned} \tag{1}$$

Finally, the results of the investigations are compared in a sensitivity matrix, where the independence of the respective sensor structures with respect to the orientation is evaluated.

3 | STRUCTURE DESIGN AND EXPERIMENTAL DATA ACQUISITION

Structures with different physical characteristics are specifically generated in order to subject them to the qualification study. A dipole characteristic in the form of a logarithmic periodic

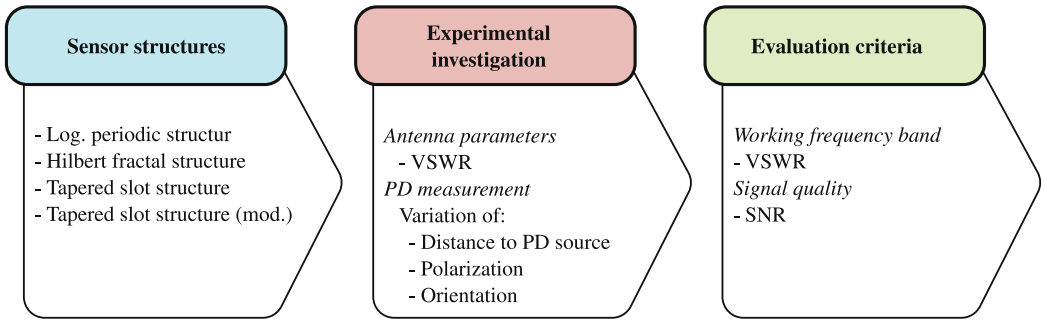

FIGURE 1 Methodical approach of the sensor qualification.

structure, a fractal structure in the form of a Hilbert fractal and two slot structures are realised. All structures are realised under the following aspects:

- working frequency band of 0.3–3 GHz,
- practical and convenient dimensions with substrate size of 20 cm × 20 cm,
- antipodal structure for orientation independent detection.

3.1 | Structure design

First, the patch antenna structures are designed and realised regarding the required working frequency band, which is set to 0.3–3 GHz. Applying the antenna structure to the dielectric results in effective wavelengths that lead to the shortening of the structures. With a relative permittivity $\varepsilon_r = 4,7$ and a height $h = 1.5$ mm of the dielectric material (FR4) and a width of the feed line $W_s = 5$ mm the effective relative permittivity according to refs. [17, 18] results in

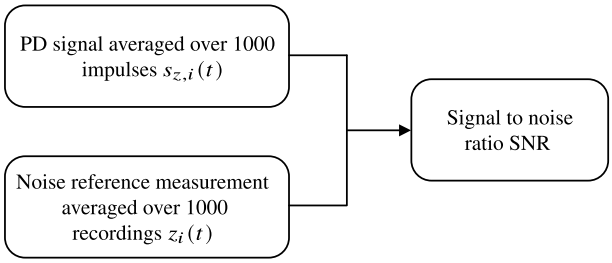

FIGURE 2 Evaluation process of the sensor structures regarding the distance, polarisation and orientation measurements.

$$\varepsilon_{r,\mathrm{eff}} = \frac{\varepsilon_r + 1}{2} + \frac{\varepsilon_r - 1}{2} \cdot \frac{1}{1 + 12 \cdot \frac{h}{W_s}} = 2.19. \tag{2}$$

Therefore, the effective maximum and minimum wavelengths are given by

$$\lambda_{\mathrm{eff}} = \frac{c_0}{f \cdot \sqrt{\varepsilon_{r,\mathrm{eff}}}} \tag{3}$$

and result in $\lambda_{\mathrm{eff,max}} = 0.676$ m and $\lambda_{\mathrm{eff,min}} = 0.068$ m for the targeted working frequency band.

In Figure 3 the investigated sensor structures are shown.

3.1.1 | Logarithmic periodic structure

Logarithmic periodic antennas are electrical $\lambda/2$ dipoles acting as active single radiators. The special arrangement results in a frequency independent impedance matching. In principle, the structure is described by a scaling factor

$$\tau = \frac{L_{n+1}}{L_n} = \frac{R_{n+1}}{R_n} = \frac{D_{n+1}}{D_n} < 1 \tag{4}$$

with $0.78 \leq \tau \leq 0.97$ and a distance factor

$$\sigma = 0.258\tau - 0.666 \tag{5}$$

with $0.13 \leq \sigma \leq 0.19$. These are set to $\tau = 0.805$ and $\sigma = 0.1417$ for the realised structure. The number of dipole elements required for the bandwidth is determined by

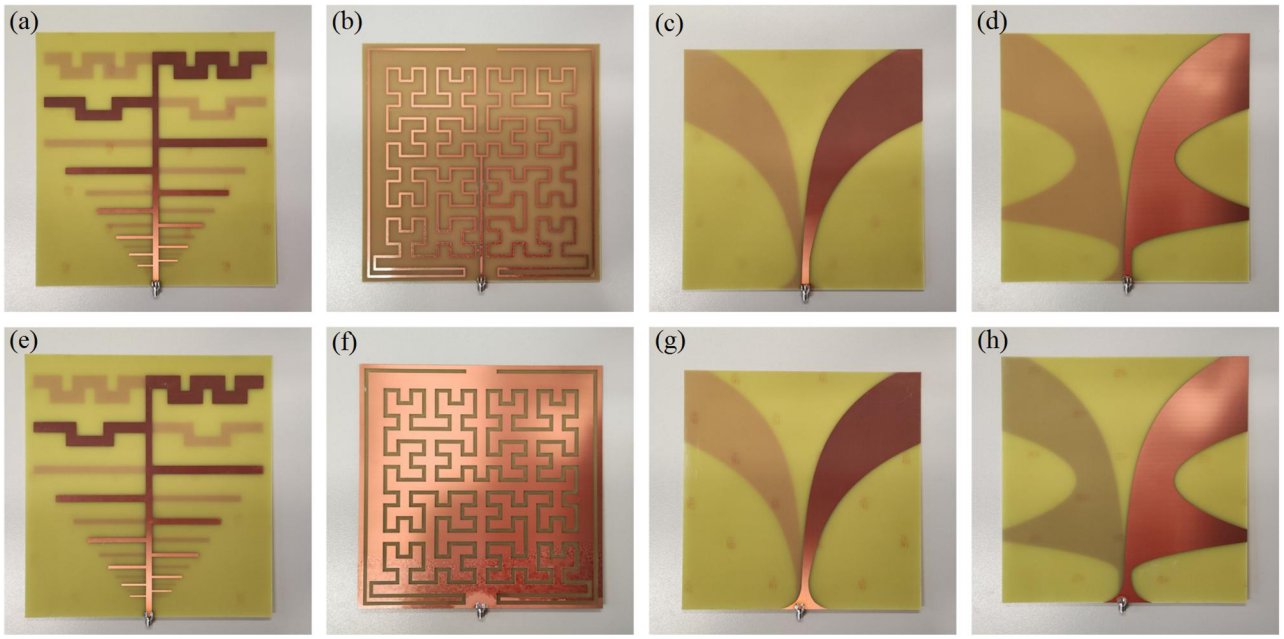

FIGURE 3 Front and back of the four different patch antenna structures; all substrates with dimensions of 20 cm × 20 cm. (a) Log. periodic—front. (b) Hilbert fractal—front. (c) Tapered slot—front. (d) Tapered slot (mod.)—front. (e) Log. periodic—back. (f) Hilbert fractal—back. (g) Tapered slot—back. (h) Tapered slot (mod.)—back.

$$N = 1 - \frac{\log \frac{L_{max}}{L_{min}}}{\log \tau} = 12. \quad (6)$$

Considering the effective wavelength, the lengths of the largest and smallest dipole are calculated as

$$L_{max} = 0.54 \cdot \lambda_{eff,max}, \quad (7)$$

$$L_{min} = \frac{\lambda_{eff,min}}{3}. \quad (8)$$

Using Equation (4), all other lengths L_n, distances R_n and thicknesses D_n of the dipole elements are obtained. The distance of the first element to the feed point is given by

$$R_{min} = \frac{L_{min}}{\arctan \alpha}, \quad (9)$$

where α determines the angle between the start point of the feed line and the alignment of the end points of the dipoles [5, 17, 18].

As shown in Figure 3, the design is antipodal. This means that the corresponding antipole is applied to the back side. This enables an omnidirectional characteristic compared to a directional characteristic of a classical logarithmic periodic antenna structure. In addition, the two longest dipole elements are designed meander-shaped and thus compressed to the length of the 10th dipole in order to reduce the dimensions of the structure.

3.1.2 | Hilbert fractal structure

Structures built like fractals allow broadband antennas by repetitions of structures as multiples of their lengths. The structure realised here consists of four Hilbert polygons of the third iteration with a feed point in the centre. The length of a basic line is 1 cm. In addition, to maximise the conductor length, almost half a turn of the outer dimensions is passed around the fractal structure on each side. The front side corresponds to an electric dipole antenna with a conductor strip thickness of 2 mm on the front side, while the back side has an inverse design. This means that a slot structure with a slot width of 3 mm corresponding to the conductor structure of the front side is implemented in a copper surface. Preliminary investigations in this context show that this approach has the advantage of approximating an omnidirectional characteristic compared to a full grounding plate. Compared to a partial grounding, there is the advantage of better matching of the structure regarding to its impedance.

3.1.3 | Tapered slot structure

Tapered slot structures are broadband slot antennas and belong to the magnetic antennas. The broadband results from the opening slot, which are described by linear, quadratic or exponential functions [18, 19]:

$$y = \pm A e^{px}. \quad (10)$$

The minimum and maximum width of the slot opening is determined by

$$W_{min} \approx \lambda_{eff,0} \quad (11)$$

and

$$W_{max} \approx \frac{\lambda_{eff,min}}{2}. \quad (12)$$

A simple tapered slot structure with a slot opening of 16 cm and a tapered slot structure modified by two additional slot openings on the sides with 8 cm width are realised.

3.2 | Measurement setup and data acquisition

To validate the structures by measurement, the antenna parameter VSWR is measured and PD pulses are recorded by the structures under real laboratory conditions.

A usual power reflection metre and a measuring probe are used for measuring the VSWR. All sensors have an SMA coaxial connector. A signal is applied to the sensor structure through this and the reflection signal, which reflects back from the structure, is measured. The frequency range is determined in steps of 5 kHz. A VSWR <2 is set as the criterion for the working frequency band.

The PD pulses are measured by the arrangement presented in Figure 4. The entire test setup and the respective patch antenna are located in a high voltage laboratory. The sensor is installed on a variable holder made of wood and only requires a connection via an ultra-low loss coaxial cable to the amplifier or oscilloscope. Figure 4a shows the realisation of the test circuit, Figure 4b focuses on the measuring cell (MC) and the sensor (S), as well as the transmission of the signals to the oscilloscope (MI). The test circuit consists of a DC voltage source and a decoupling impedance Z_d to protect the source in case of a breakdown. A PD measuring circuit in accordance with the IEC 60270 standard is also integrated. This consists of a coupling capacitor C_k in parallel with the device under test, which in this case is the measuring cell (MC), and a PD measuring system[1] (MS) connected via a CQ. In case of a PD in the device under test (MC), a charge displacement occurs within the coupling capacitance C_k, which in turn is recorded by the PD MS. In a connected evaluation software[2] a charge quantity is determined in accordance with the IEC 60270 standard. In terms of the standard, the MS is narrowband with

[1]Omicron electronics GmbH, Typ MPD 600.
[2]Omicron electronics GmbH, MPD/MI Software.

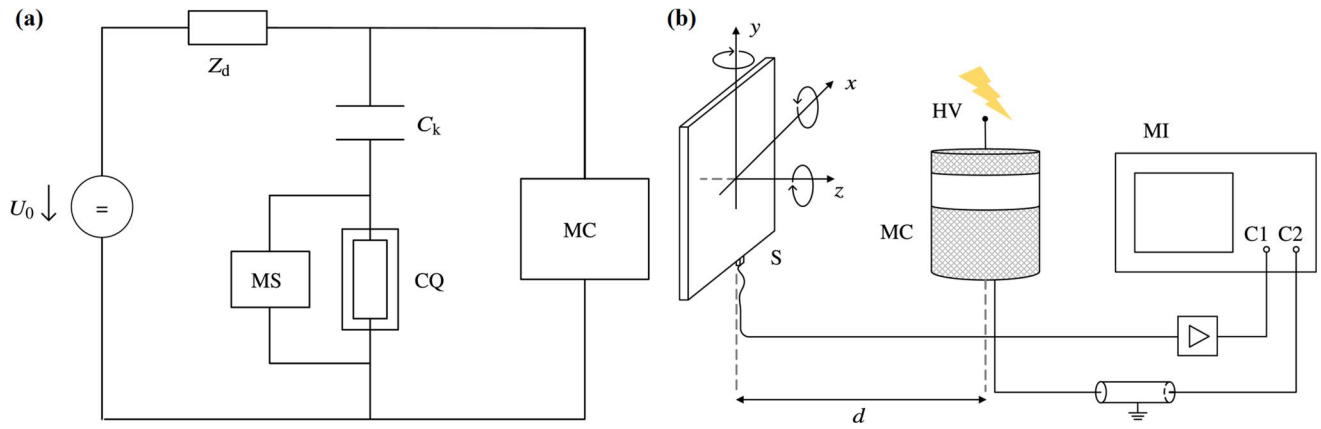

FIGURE 4 Measurement setup. (a) Test circuit with high voltage U_0, decoupling impedance Z_d, coupling quadripole (CQ) for the partial discharge (PD) measuring system (MS) and measuring cell (MC). (b) Orientation and rotation direction of the sensors (S) in distance d to the PD source in the measuring cell (MC) with amplifier (V) and oscilloscope (MI), shown is initial position.

a bandwidth of 300 kHz and a centre frequency of 250 kHz. The system is used to achieve comparable charge levels of approximately 40 pC. For this purpose, a negative DC voltage is varied in a range from −4.4 kV to −5.0 kV until the target charge level is reached. A comparability, for example, between the charge level according to IEC 60270 and the amplitude of the signals recorded with the patch antennas, is not possible due to the narrow bandwidth of the measuring circuit according to IEC 60270 and the broadband capability of the sensors.

The measuring cell (MC) is used and presented in preliminary work for reflectionfree and broadband acquisition of PD impulses in refs. [20, 21]. Inside the measurement cell (MC), a needle is located opposite a ground electrode to which the high voltage (HV) is applied to generate corona PD pulses. The cell itself is conical in shape and thus has a characteristic impedance of 50 Ω. The resulting PD current is decoupled at the earth electrode at the lower end of the measuring cell using a coaxial cable. As part of the qualification of the patch antennas, this signal is used as a trigger on channel 1 (C1) to start the recording of a PD pulse. The oscilloscope (MI) starts a 1 µs recording for each PD pulse and saves the sequence. The recording is carried out time synchronously on C1 and channel 2 (C2) to which the patch sensor is connected. The result is a data matrix per channel with 1000 columns in which each column corresponds to a PD. This enables signal averaging over 1000 recordings in order to minimise interference. The measuring cell consists in parts of polymer shown as a white ring in Figure 4b, so that the electromagnetic signal is coupled out and detectable by the sensors. The sensor (S) with the respective structure is connected to the oscilloscope (MI) by a low loss 50 Ω cable and a broadband amplifier with an impedance of 50 Ω over the relevant frequency range. The oscilloscope has an analogue bandwidth of 4 GHz and a sampling frequency of 20 GHz.

The orientation shown in Figure 4b is the initial position of the sensor, from which the sensor is rotated around the respective axes to represent the application relevant investigation of the orientation dependence of the detection of PD by the sensor structures. Orientation in this case is counted as the distance, polarisation and angle and rotation to the PD source. The distance investigation is done by varying the distance d to the PD source in initial position. The polarisation investigation is done on the one hand by rotation around the z-axis, which is in plumb line to the PD source. Another polarisation measurement is performed with the y-axis in plumb to the PD source and rotation around the same. All sensors are linearly polarised, which means that a damping of the signal is expected depending on the vertical and horizontal orientation. Rotation around the x- and y-axis additionally investigates the omnidirectional characteristic. Under real test conditions, the location of origin of the PD is not known, so a detection that is independent of the orientation to the PD source is desirable.

As already mentioned, 1000 PD pulses are recorded in each position and in post-processing the average value over these 1000 PD pulses is determined. This is possible by triggering on the conducted PD signal of the measuring cell and then starting time synchronous recording on all channels. A time window for the recording duration is determined beforehand by displaying the measurement signal from the measuring cell, which ensures the exclusive recording of a single pulse per recording sequence. As a result, the test setup with measuring cell enables a reproducible test procedure for qualifying the sensors. In addition, a corresponding interference reference measurement is performed in each positioning, to calculate the SNR according to Equation (1) as part of the evaluation of the structures. The interference reference environment is also averaged, whereby the remaining interference component is represented despite the averaging of the signal. The interference environment includes ambient noise, narrowband interferers such as radio band, Wlan etc. and also broadband interference pulses such as those emitted by power electronic switches. By averaging the signal, interferers that statistically do not occur at the same repetition frequency as the partial interference are averaged out. In addition, this reduces the

ambient noise. Furthermore, averaging 1000 PD produces a reliable result for the SNR.

4 | RESULTS AND DISCUSSION

4.1 | Operating frequency bands

In Figure 5 the results of the measurement of the VSWR are shown. The criterion for the working frequency range is a target value for the VSWR of <2. The measurement defines the working frequency bands listed in Table 1. All structures have only one working frequency band, tolerating up to 3 consecutive values of VSWR >2 and < 3 not leading to division into several working frequency bands.

The logarithmic periodic structure provides a VSWR <2 already from 590 MHz, which corresponds to the lowest subfrequency of the working frequency bands of all sensors. In contrast, the VSWR at frequencies below 590 MHz is in some cases twice as high compared to the other structures investigated. For the Hilbert fractal structure, the VSWR from a frequency of 610 MHz is below a level of 2 with a few outliers and shows a VSWR slightly above two in lower frequencies, especially in direct comparison with the logarithmic periodic structure. This is in principle positively evaluated, since relevant parts of the PD signals lie also in frequency ranges below 300 MHz, which are only slightly affected in the scope of the measurement due to this under use of the Hilbert structure. The tapered slot structure shows a VSWR <2 of 830 MHz, which means that the lower frequency of the working band deviates significantly from the target value 300 MHz. In contrast, the modified tapered slot structure extended by two more slots has a lower frequency of the working frequency band of 725 MHz. The modification thus achieves an extension of the working frequency band by approximately 100 MHz downwards.

4.2 | PD measurements

In Figure 6 the PD pulses measured by the corresponding structures in initial position and 1.5 m distance are shown. These represent the average of 1000 measured PD pulses. It shows that for a comparable charge level, the simple tapered slot structure has a signal level that is higher by a factor of about 2. However, this also occurs with the after-reflections and other disturbances which are not free of mean values.

The frequency spectra of the signals in Figure 6 are shown in Figure 7. The integral $\int |S(f)|$ of the one sided frequency spectrum normalised to one is shown in order to establish comparability between the frequency spectra of the acquired signals. The frequency spectrum of the signal, which is

TABLE 1 Operating frequency bands of the different structures based on voltage standing wave ratio.

Patch antenna structures	Band	Frequency range (MHz)
Log. periodic structure	1	590–3000
Hilbert fractal structure	1	610–3000
Tapered slot structure	1	830–3000
Tapered slot structure (mod.)	1	725–3000

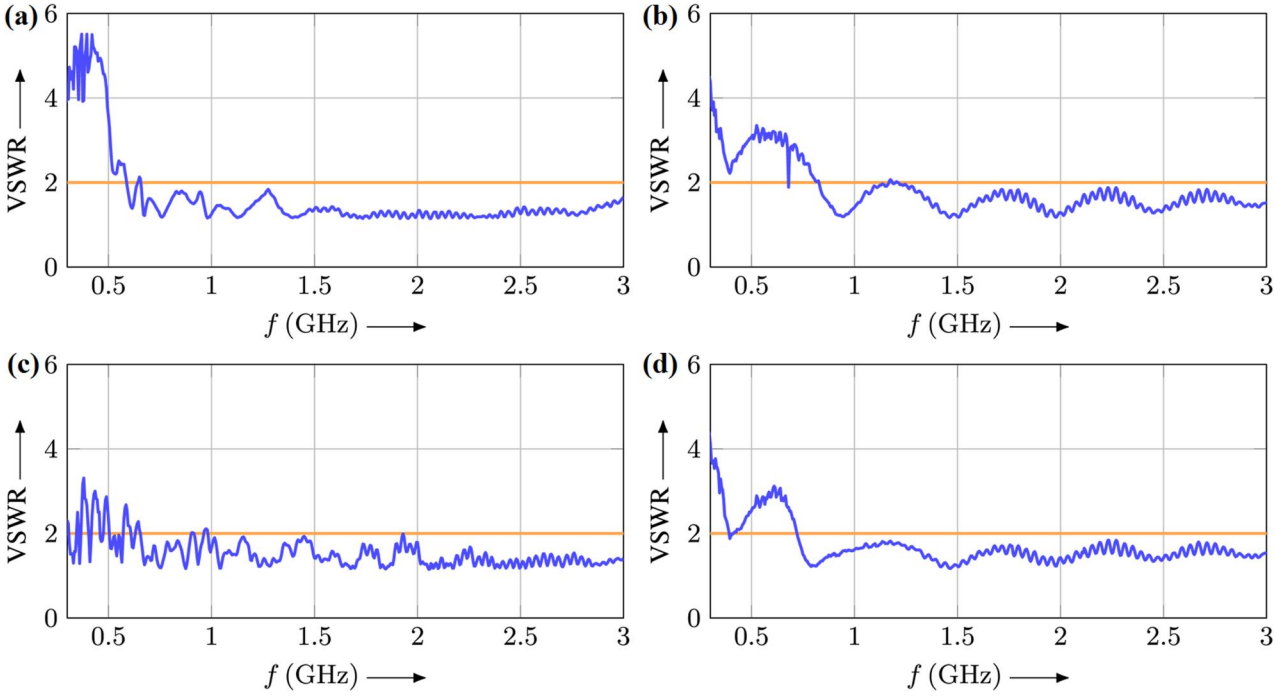

FIGURE 5 Voltage standing wave ratio of the different sensor structures. (a) Log. periodic structure. (b) Tapered slot structure. (c) Hilbert fractal structure. (d) Tapered slot structure (mod.).

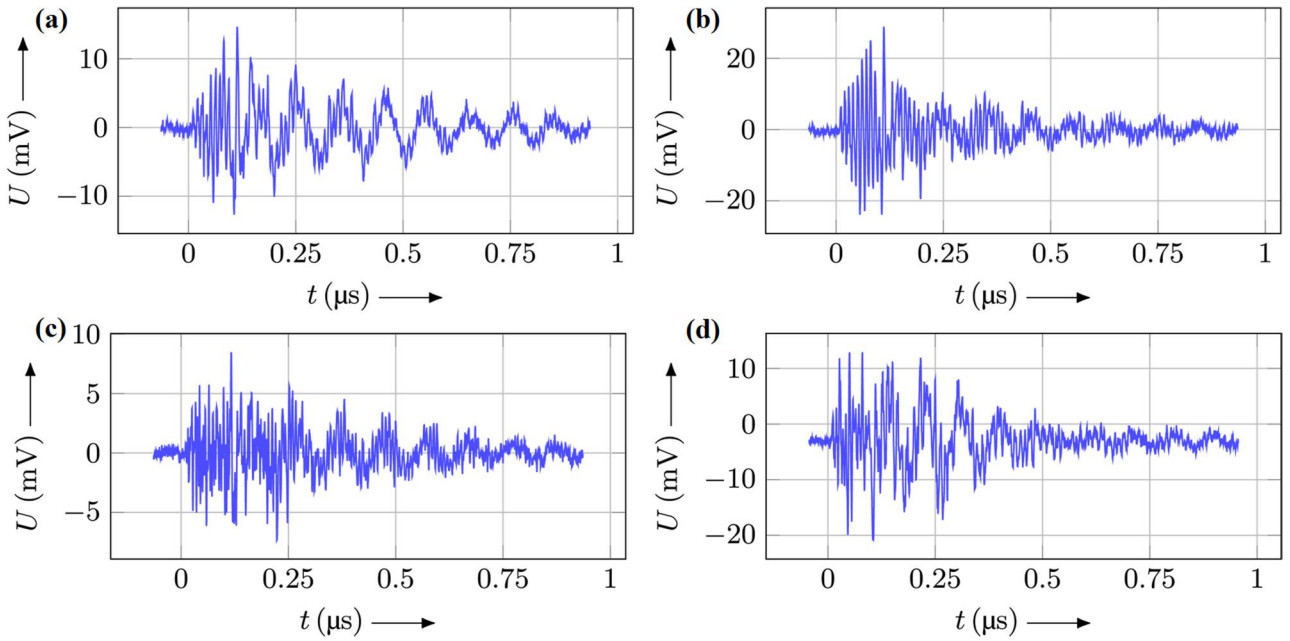

FIGURE 6 Time signals of the different sensors averaged over 1000 detected partial discharge (PD)—sensors aligned at 1.5 m distance with z-axis in plumb line with PD source (cf. Figure 4b). (a) Log. periodic structure. (b) Tapered slot structure. (c) Hilbert fractal structure. (d) Tapered slot structure (mod.).

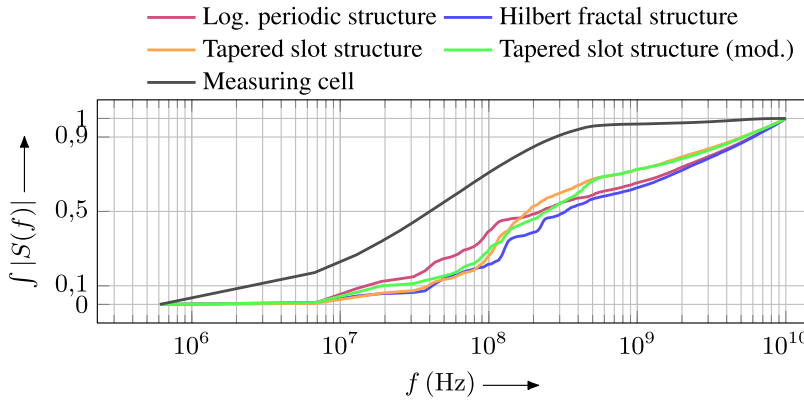

FIGURE 7 Integrals of the normalised frequency spectrum of the measured partial discharge (PD), each averaged over 1000 PD pulses, recorded with the patch sensors and decoupled from the measuring cell via a coaxial cable for comparison - sensors aligned at 1.5 m distance with z-axis in plumb line with PD source (cf. Figure 4b).

measured broadband without reflection from the measuring cell using a coaxial cable, is also shown. The associated time signal corresponds to a trichel pulse and is analysed in detail in refs. [20, 21]. It is visible that the frequency ranges of the time signals recorded by the patch antennas correspond to the signal from the measuring cell. The signals recorded with the patch antennas do not contain any frequency components below 7 MHz, which results in a deviation of the frequency spectra of the patch antennas compared to the signal from the measuring cell. It is important to note that the geometric layout of the sensors is designed for a lower target frequency of 300 MHz. The measurement of the VSWR results in slightly upwards shifted lower frequencies of the working frequency band according to Table 1. Frequency components below this lower frequency limit are still detected, but are reflected more strongly at the coaxial connector due to the mismatch of the impedance in this frequency range as shown in Figure 5. As a result, frequency components up to a lower frequency of 7 MHz are visible in the frequency spectrum of the signals detected by the patch antennas.

Since with the help of the time signals and frequency spectra only a check with regard to a general pulse detection is possible, the SNR is presented in Tables 2–4. The distance investigation concerning the logarithmic periodic structure and the simple tapered slot structure results in a decreasing SNR with distance. This corresponds to the expectations that the signal energy decreases with the distance. The distance investigation concerning the Hilbert structure results in an increase of the SNR. The structure has both an electric and a magnetic dipole structure, so that a possible reason for the increase in

SNR is that in the distance investigation the far field is approached with increasing distance for more and more frequencies. Accordingly, further investigations are suggested for this structure. The modified tapered slot structure shows a non-uniform behaviour in the distance investigation. This structure has a slot structure on three edges, which causes reflections or stronger interferers that are not free of mean values to couple in. Further investigations are recommended to this effect as well. In general, all structures are suitable for measurements in the investigated distance range and qualify for investigations with larger distances.

The logarithmic periodic structure and the Hilbert structure do not indicate a clear preferential polarisation with respect to the *z*-axis, since the copper structures are distributed both vertically and horizontally here. The preferred polarisation of the modified tapered slot structure is 90°. Since this structure has a slot opening on three edges, a different preferred polarisation than the simple tapered slot structure with 180° is plausible. Both the simple tapered slot structure and modified tapered slot structure show a higher SNR at 0° and 180° respectively. However, since these polarisations are expected to have comparable SNR, further investigations are recommended in this regard.

TABLE 2 Signal to noise ratio in dB of distance investigation: *z*-axis in plumb line in initial position (cf. Figure 4b).

	Signal to noise ratio (dB)		
Patch antenna structures	$d = 1.5$ m	$d = 2.1$ m	$d = 2.9$ m
Log. periodic structure	9.732	7.683	3.581
Hilbert fractal structure	7.707	9.006	15.880
Tapered slot structure	13.060	9.942	7.676
Tapered slot structure (mod.)	13.671	37.904	27.548

In the context of the polarisation investigation around the *y*-axis, again no preferential polarisation is shown for the Hilbert fractal. Also for the modified tapered slot structure there is no significant preferential polarisation. The logarithmic periodic structure and the tapered slot structure exhibit preferential polarisation at 0°. This correlates with the alignment of a classical antenna structure according to these structures as a directional antenna in vertical positioning. A deviation between the simple and modified tapered slot structure is caused by the additional slot openings at two additional edges.

Regarding the orientation measurement, a similarity between the orientation in initial position (0° | 0°) and the rotation around the *y*-axis by 180° starting from the initial position is expected due to the antipodal structure. This is valid for the Hilbert structure as well as for the modified tapered slot structure. An orientation around 45° | −45° and around −45° | 135° also suggests similar results considering an approximation to the omnidirectional characteristic. This is also true for Hilbert structure and modified tapered slot structure in this case.

In Table 5 an evaluation matrix concerning the investigated structures is presented in form of a table. The evaluation of the sensitivity represents, on the one hand, the frequency behaviour and, on the other hand, the approximation to an omnidirectional characteristic. The evaluation takes into account that the SNR is logarithmically scaled. The non-logarithmic SNR values are each related to the maximum value of the respective measurement series for each structure. For the orientation measurement, the value is related to the comparable orientation. For a 0° | 0° orientation, values are expected to be similar to those of 0° | 180° orientation. With regard to the 45° | −45° orientation, the −45° | 135° orientation is used as a comparison. If the determined values of the SNR of the measurement series vary such that a similarity of the values is less than 0.2, the structure is considered to be highly sensitive to the respective parameter. If a tendency or comparability is physically to be expected, to which

TABLE 3 Signal to noise ratio in dB of polarisation investigation: *z*-axis or *y*-axis in plumb line (cf. Figure 4b), rotation clockwise. Initial position for *y*-axis polarisation is a vertical alignment of the sensor.

	Signal to noise ratio at *z*-axis (dB)			Signal to noise ratio in *y*-axis (dB)		
Patch antenna structures	**0°**	**90°**	**180°**	**0°**	**45°**	**90°**
Log. periodic structure	6.089	4.835	6.127	47.509	36.119	30.674
Hilbert fractal structure	7.322	6.024	7.025	22.308	20.407	21.682
Tapered slot structure	7.317	5.616	18.260	28.048	14.742	13.874
Tapered slot structure (mod.)	17.074	22.992	6.787	40.832	44.567	40.425

TABLE 4 Signal to noise ratio in dB of orientation study: *z*-axis in plumb line (cf. Figure 4b), rotation clockwise first around *y*-axis, then around *x*-axis.

	Signal to noise ratio at *y*-axis | *x*-axis (dB)			
Patch antenna structures	**0° | 0°**	**0° | 180°**	**45° | −45°**	**−45° | 135°**
Log. periodic structure	24.548	34.865	24.798	29.266
Hilbert fractal structure	16.243	15.589	16.009	17.787
Tapered slot structure	29.545	45.450	41.407	36.302
Tapered slot structure (mod.)	38.618	35.949	15.476	14.200

TABLE 5 Sensitivity of the structures to distance, polarisation, orientation and frequency.

Patch antenna structures	Sensitivity to				Frequency bands	Lower frequency
	Distance	Polarization z-axis	Polarization y-axis	Orientation		
Log. periodic structure	low	low	moderate	moderate	1	590 MHz
Hilbert fractal structure	moderate	low	moderate	low	1	610 MHz
Tapered slot structure	low	high	moderate	high	1	830 MHz
Tapered slot structure (mod.)	high	high	moderate	moderate	1	725 MHz

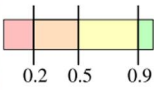

the results contradict, this leads to an additional devaluation. This is the case, for example, if there are significant differences between the results of the polarisation measurement around the z-axis for 0° and 180°, since a correspondence is expected here. If there is a similarity of the values in the range of a factor from 0.9 to 1, a low sensitivity of the structure to the respective parameter is considered. Furthermore, with regard to the frequency matching of the structure, the lowest frequency of the working frequency band, which is determined by the VSWR, is taken into account.

Within the study, the logarithmic periodic structure and the Hilbert fractal structure proved to be particularly suitable with respect to the requirements of frequency and independence of orientation. These structures qualify for further investigations regarding calibration and aspects like correction factors. The tapered slot structures prove to be less suitable according to the applied evaluation standards. Further investigation and optimisation are required here.

5 | CONCLUSION AND OUTLOOK

In the context of contactless broadband and orientation independent detection of PD the developed structures are suitable. As verified in the studies they all provide the advantage that the knowledge of the location of the origin of the PD is not required and ensure a high information content of the signal due to their proven broadband working frequency bands. In addition to the fundamental suitability of all structures, the following main points result from the investigative studies:

- The realised structures have a continuous working frequency band.
- The realised logarithmic periodic structure and the Hilbert fractal structure have the lowest sub frequency of the working frequency bands.
- The time signals recorded with the realised structures have a comparable frequency spectrum to the broadband and reflection free recorded signal from the measuring cell.
- The realised structures detect PD in each orientation with an SNR >1.
- In terms of sensitivity to alignment, the logarithmic periodic structure and the Hilbert fractal structure prove to be particularly robust.

Further aspects to be investigated are in particular the variation of the distance and the height of the structure in relation to the PD source. The determination of the maximum reach of the structures is particularly relevant with respect to the application relevance. A higher discretisation in the distance variation as well as a variation of the apparent charge is useful in the context of a signal estimation and correction function. Supporting a simulation of the circular radiation characteristic and the gain is useful.

Another aspect is the measurement of PD without the trigger of the measuring cell, as this trigger is not present during on-site use. Initial investigations show that the PD are still able to be recorded. The signal from the measuring cell is also recorded here as a control. However, a suppression method is necessary, especially in the case of strong interference environments. This is the subject of the work currently being carried out.

ACKNOWLEDGEMENTS

This project was funded by the TU Dortmund University.

Open Access funding enabled and organized by Projekt DEAL.

NOMENCLATURE

Abbreviation

FR4	composite material consisting of epoxy resin and glass fiber fabric
PD	partial discharges
RL	return loss
SNR	signal to noise ratio
UHF	ultra high frequency
VHF	very high frequency
VSWR	voltage standing wave ratio

Symbol

A	stretch factor of the e-function
c_0	velocity of light in m/s
D_n	thickness of the nth dipole element in m
d	distance to PD source in m
f	frequency in Hz
h	height of the substrate in m
L_{max}	length of a longest dipole element in m
L_{min}	length of a shortest dipole element in m

L_n length of the nth dipole element in m
N number of dipole elements
p compression factor of the e-function
R_{min} distance from feed point to shortest dipole element in m
R_n distance from feed point to nth dipole element in m
$s_i(t)$ sampled PD time signal without interference components (useful signal) in V
$s_{z,i}(t)$ sampled PD time signal with interference components in V
W_{max} maximum width of the slot opening in m
W_{min} minimum width of the slot opening in m
W_s width of the feed line in m
$z_i(t)$ measured noise and interference signal in V
α gradient angle between feed point and longest dipole element in °
ε_r relative permittivity
$\varepsilon_{r,eff}$ effective relative permittivity
$\lambda_{eff,max}$ largest effective wavelength in m
$\lambda_{eff,min}$ smallest effective wavelength in m
$\lambda_{eff,0}$ center frequency in m
σ distance factor
τ scaling factor

CONFLICT OF INTEREST STATEMENT

The authors declare no conflicts of interest.

DATA AVAILABILITY STATEMENT

The data that support the findings of this study are available from the corresponding author, upon reasonable request.

ORCID

Kerstin Friebe https://orcid.org/0000-0002-7947-4342

REFERENCES

1. DIN EN 60270 (VDE 0434). Hochspannungs-Prüftechnik: Teilentladungsmessungen (2016)
2. Küchler, A.: Hochspannungstechnik: Grundlagen - Technologie - Anwendungen, 4. Auflage. Springer Berlin Heidelberg, Berlin (2017)
3. Schon, K.: Hochspannungsmesstechnik: Grundlagen – Messgeräte – Messverfahren. Springer Fachmedien Wiesbaden, Wiesbaden (2016)
4. Schwab, A.J., Kürner, W., Verträglichkeit, E.: 6. bearbeitete und ergänzte Auflage. Springer Berlin Heidelberg, Berlin (2011)
5. Pawar, S.S., Shandilya, M., Chaurasia, V.: Parametric evaluation of microstrip log periodic dipole array antenna using transmission line equivalent circuit. Eng. Sci. Technol. Int. J. 20(4), 1260–1274 (2017)
6. Kong, X., et al.: An Improved Vivaldi antenna for the UHF partial discharge detection. In: 2022 IEEE 4th International Conference on Dielectrics (ICD), Palermo, Italy, pp. 253–256 (2022)
7. Uwiringiyimana, J.P., Suwarno, Khayam, U.: Design of an ultra-wide band microstrip patch antenna for partial discharge detection on power transformer. In: 2021 IEEE International Conference on the Properties and Applications of Dielectric Materials (ICPADM), Johor Bahru, Malaysia, pp. 242–245 (2021)
8. Darwish, A., et al.: A coplanar waveguide based antenna for partial discharge detection in gas-insulated switchgear. In: 2022 3rd International Conference on Smart Grid and Renewable Energy (SGRE). Doha, Qatar, pp. 1–5 (2022)
9. Wu, Q., et al.: The study of Archimedean spiral antenna for partial discharge measurement. In: 2013 Fourth International Conference on Intelligent Control and Information Processing (ICICIP), Beijing, China, pp. 694–698 (2013)
10. Jin, Z., et al.: Two types of compact UHF antennas for partial discharge measurement. In: 2008 International Conference on High Voltage Engineering and Application, Chongqing, China, pp. 616–620 (2008)
11. Cui, Z., et al.: Wideband UHF antenna for partial discharge detection. Appl. Sci. 10(5), 1698 (2020)
12. Zahed, A.A., et al.: Comparison of different fourth order Hilbert fractal antennas for partial discharge measurement. IEEE Trans. Dielectr. Electr. Insul. 24(1), 175–182 (2017)
13. Li, J., et al.: UHF stacked Hilbert antenna array for partial discharge detection. IEEE Trans. Antenn. Propag. 61(11), 5798–5801 (2013)
14. Wu, T., et al.: Design of partial discharge UHF microstrip antenna based on LS Peano fractal structure. In: 2021 IEEE 5th Information Technology,Networking,Electronic and Automation Control Conference (ITNEC), Xi'an, China, pp. 556–560 (2021)
15. Suryandi, A.A., Khayam, U.: New designed bowtie antenna with middle sliced modification as UHF sensor for partial discharge measurement. In: 2014 International Conference on Smart Green Technology in Electrical and Information Systems (ICSGTEIS), Kuta, Bali, Indonesia, pp. 98–101 (2014)
16. Rhamdhani, T., Khayam, U., Zaeni, A.: Improving antenna performance by combining dipole and bowtie antenna for partial discharge measurement in gas insulated switchgear. In: 2022 IEEE International Conference in Power Engineering Application (ICPEA), Shah Alam, Malaysia, pp. 1–4 (2022)
17. Kark, K.W.: Antennen und Strahlungsfelder: Elektromagnetische Wellen auf Leitungen, im Freiraum und ihre Abstrahlung, 8. Auflage. Springer Fachmedien Wiesbaden, Wiesbaden (2020)
18. Balanis, C.A.: Antenna Theory. 4. Wiley Global Research (STMS), Auflage (2015)
19. Chen, Z.N., et al.: Handbook of Antenna Technologies. Springer Singapore (2016)
20. Lühring, U., Wienold, D., Jenau, F.: Comparative investigation on pulse shape parameters of partial discharges in air under AC and DC voltage stress. In: 2016 51st International Universities Power Engineering Conference (UPEC), Coimbra, Portugal, pp. 1–4 (2016)
21. Lühring, U., Wienold, D., Jenau, F.: Investigation on the pulse shape of DC corona discharges in air under varying test voltage level. In: 2018 IEEE 2nd International Conference on Dielectrics (ICD), Budapest, Hungary, pp. 1–6 (2018)

How to cite this article: Friebe, K., Jenau, F.: Experimental qualification and sensitivity study of antipodal patch antenna structures for orientation independent detection of partial discharges. High Voltage. 9(3), 674–684 (2024). https://doi.org/10.1049/hve2.12434